
Accelerated Article Preview

High genetic barrier to SARS-CoV-2 polyclonal neutralizing antibody escape

Received: 1 July 2021

Accepted: 7 September 2021

Accelerated Article Preview Published
online 20 September 2021

Cite this article as: Schmidt, F. et al. High genetic barrier to SARS-CoV-2 polyclonal neutralizing antibody escape. *Nature* <https://doi.org/10.1038/s41586-021-04005-0> (2021).

Fabian Schmidt, Yiska Weisblum, Magdalena Rutkowska, Daniel Poston, Justin Da Silva, Fengwen Zhang, Eva Bednarski, Alice Cho, Dennis J. Schaefer-Babajew, Christian Gaebler, Marina Caskey, Michel C. Nussenzweig, Theodora Hatziioannou & Paul D. Bieniasz

This is a PDF file of a peer-reviewed paper that has been accepted for publication. Although unedited, the content has been subjected to preliminary formatting. Nature is providing this early version of the typeset paper as a service to our authors and readers. The text and figures will undergo copyediting and a proof review before the paper is published in its final form. Please note that during the production process errors may be discovered which could affect the content, and all legal disclaimers apply.

High genetic barrier to SARS-CoV-2 polyclonal neutralizing antibody escape

<https://doi.org/10.1038/s41586-021-04005-0>

Received: 1 July 2021

Accepted: 7 September 2021

Published online: 20 September 2021

Fabian Schmidt^{1,4}, Yiska Weisblum^{1,4}, Magdalena Rutkowska³, Daniel Poston¹, Justin Da Silva¹, Fengwen Zhang¹, Eva Bednarski¹, Alice Cho², Dennis J. Schaefer-Babajew², Christian Gaebler², Marina Caskey², Michel C. Nussenzweig^{2,3}, Theodora Hatzioannou¹✉ & Paul D. Bieniasz^{1,3}✉

The number and variability of the neutralizing epitopes targeted by polyclonal antibodies in SARS-CoV-2 convalescent and vaccinated individuals are key determinants of neutralization breadth and the genetic barrier to viral escape^{1–4}. Using HIV-1 pseudotypes and plasma-selection experiments with vesicular stomatitis virus/SARS-CoV-2 chimeras⁵, we show that multiple neutralizing epitopes, within and outside the receptor binding domain (RBD), are variably targeted by human polyclonal antibodies. Antibody targets coincide with spike sequences that are enriched for diversity in natural SARS-CoV-2 populations. By combining plasma-selected spike substitutions, we generated synthetic ‘polymutant’ spike protein pseudotypes that resisted polyclonal antibody neutralization to a similar degree as circulating variants of concern (VOC). By aggregating VOC-associated and antibody-selected spike substitutions into a single polymutant spike protein, we show that 20 naturally occurring mutations in SARS-CoV-2 spike are sufficient to generate pseudotypes with near-complete resistance to the polyclonal neutralizing antibodies generated by convalescents or mRNA vaccine recipients. Strikingly, however, plasma from individuals who had been infected and subsequently received mRNA vaccination, neutralized pseudotypes bearing this highly resistant SARS-CoV-2 polymutant spike, or diverse sarbecovirus spike proteins. Thus, optimally elicited human polyclonal antibodies against SARS-CoV-2 should be resilient to substantial future SARS-CoV-2 variation and may confer protection against potential future sarbecovirus pandemics.

Neutralizing antibodies elicited by prior infection or by vaccination likely represent a key component of protective immunity against SARS-CoV-2. Antibodies targeting the receptor binding domain (RBD) of the spike protein are thought to dominate the neutralizing activity of convalescent or vaccine recipient plasma⁶, and include the most potent neutralizing antibodies cloned from convalescent individuals^{7–11}. Nevertheless, additional SARS-CoV-2 neutralizing antibody targets include the N-terminal domain (NTD) and the fusion machinery^{4,8,10,12,13}, and the full spectrum of epitopes targeted by neutralizing antibodies in convalescent or vaccine recipient plasma has not been defined. SARS-CoV-2 variants of concern (VOC) or variants of interest (VOI) encode spike amino acid substitutions^{14–17}, some of which confer resistance to individual human monoclonal antibodies but have variable, typically modest, effects on neutralization by polyclonal plasma antibodies^{1,6,9,17–20}. Mutated sites in VOCs include those in the RBD, NTD and elsewhere, but the numbers and locations of spike substitutions required for SARS-CoV-2 to evade the polyclonal neutralizing antibodies encountered in vaccine recipients or convalescents is unknown and is a crucial determinant of population immunity.

Polyclonal neutralizing antibody targets

Exploiting the fact that SARS-CoV is poorly neutralized by SARS-CoV-2 convalescent plasma, we compared the sensitivity of HIV-1 pseudotypes bearing parental and chimeric spike proteins in which RBD sequences were exchanged (SARS-CoV-2(1-RBD) and SARS-CoV(2-RBD), Fig. 1a, Extended Data Fig. 1) to neutralization by plasma from 26 individuals from a previously described Rockefeller University COVID19 convalescent cohort²¹. The plasma samples were obtained at an average of 1.3 months after infection and were selected for high SARS-CoV-2 neutralization titers (RU27 plasma panel). Compared to the SARS-CoV-2 pseudotype, the SARS-CoV-2(1-RBD) pseudotype was less sensitive to neutralization by 21/26 plasmas (median difference = 1.8-fold, range 0.5 to 9.8-fold, $p=0.0005$ (Wilcoxon 2-tailed test), Fig. 1b). Conversely the SARS-CoV(2-RBD) pseudotype was more sensitive than the SARS-CoV pseudotype to all plasmas (median difference 8-fold, range 1.2 to 75.5 fold, $p<0.0001$ (Wilcoxon 2-tailed test), Fig. 1c). Nevertheless, the neutralizing potency of some plasmas was hardly affected when the SARS-CoV-2 RBD was replaced by the SARS-CoV RBD, even though some of those plasmas were minimally active against SARS-CoV (e.g. RU9, RU10, RU11,

¹Laboratory of Retrovirology, The Rockefeller University, New York, NY, USA. ²Laboratory of Molecular Immunology, The Rockefeller University, New York, NY, USA. ³Howard Hughes Medical Institute, The Rockefeller University, New York, NY, USA. ⁴These authors contributed equally: Fabian Schmidt, Yiska Weisblum. ✉e-mail: thatzio@rockefeller.edu; pbieniasz@rockefeller.edu

RU15 Fig. 1b, c). Indeed, plasmas that poorly neutralized SARS-CoV-2 potentially neutralized chimeric spike pseudotypes with either RBD or the other spike domains from SARS-CoV-2 (Fig. 1b, c). For the plasma panel as a whole, pseudotype neutralizing potency against SARS-CoV-2 did not correlate with potency against SARS-CoV or SARS-CoV-2(1-RBD) but did correlate with potency against SARS-CoV(2-RBD) (Extended Data Fig. 2a,b,c). Although altered RBD conformation in chimeric spike proteins might affect neutralization, these data indicate that while the RBD constitutes a major neutralizing target, substantial plasma neutralizing activity is also directed against non-RBD epitopes.

Polyclonal antibody-selected variants

To more precisely map the targets of polyclonal neutralizing antibodies in convalescent individuals, we passaged a rVSV/SARS-CoV-2 chimeric virus^{1,5} in the presence of each of the RU27 plasmas for up to six passages. Importantly, rVSV/SARS-CoV-2 mimics the neutralization properties of SARS-CoV-2^{1,5} but obviates the safety concerns that would accompany such studies with authentic SARS-CoV-2. NGS sequencing indicated that rVSV/SARS-CoV-2 passage in 22 out of the 27 plasmas led to the selection of spike mutants (Fig. 2a, Extended Data Fig. 3, Table S1). For some plasmas, multiple substitutions were selected at distinct but proximal sites in viral subpopulations, indicating a dominant neutralizing activity targeting a particular epitope. For other plasmas, substitutions were enriched in multiple regions of the spike coding sequence, suggesting co-dominant neutralizing activities. Six passages rVSV/SARS-CoV-2 without plasma enriched a small number of substitutions that were assumed to represent cell-culture or fitness-enhancing adaptations (e.g. T604I) but were distinct from the majority of substitutions arising after rVSV/SARS-CoV-2 passage in plasma (Extended Data Fig. 3, Table S1). Cumulatively, the plasma-selected mutations were enriched in specific elements within NTD, RBD and other spike domains (Fig. 2a, Table S1). From the 27 plasma-passaged virus populations, 38 individual mutant viruses were isolated by plaque purification; each encoded one, two or three spike substitutions (Fig. 2b) that generally occurred at high frequency in the passaged viral populations (Table S1).

We compared the distribution of mutations selected by rVSV/SARS-CoV-2 passage with the RU27 plasma panel with those occurring in circulating SARS-CoV-2 populations (Fig. 2a-d). In both plasma-selected and naturally occurring sequences, substitutions were enriched in several elements that contribute to the 'supersite' targeted by NTD-binding neutralizing antibodies^{12,13} (Fig. 2a-d). Similar plasma-selected and natural sequence variation was also evident in elements targeted by class 2 and class 3 RBD-binding neutralizing antibodies²². Mutations known to confer resistance to class I RBD antibodies were not selected by plasma passage, perhaps reflecting a lower than expected abundance of class I antibodies in this plasma panel (Fig. 2a-d). Other sites, including spike amino acids -680-700 and -930 exhibited variation in both plasma-passaged and natural variant datasets, but have not yet been demonstrated to be targeted by neutralizing antibodies. Nevertheless, the similarity in the distribution of natural and plasma-selected sequence variation within spike suggests that selection by neutralizing antibodies is a driver of divergence in circulating SARS-CoV-2 populations.

Of the 38 plaque-purified rVSV/SARS-CoV-2 mutants recovered following passage in RU27 plasmas, 34 exhibited varying degrees of reduced sensitivity to neutralization by the plasma that was used for its selection (median 3.1 fold reduced NT₅₀, range 0.8 to 39.3 fold, Extended Data Fig. 4, 5). Nevertheless, for 37/38 of the selected rVSV/SARS-CoV-2 mutants, the selecting plasma exhibited residual neutralizing activity. We aggregated 13 mutations from the plasma selected viruses based on their effects on plasma neutralization sensitivity (Extended Data Fig. 4, 5) and distribution throughout the spike protein, generating a single synthetic 'polymutant' spike (PMS) protein sequence, termed PMS1-1 (Extended Data Fig. 6a). An rVSV/SARS-CoV-2 derivative encoding

these spike mutations (rVSV/SARS-CoV-2_{PMS1-1}) exhibited resistance to neutralization by the RU27 plasma panel that was greater in magnitude and consistency than the individual plasma selected mutants (median 8.0-fold, range 2.7 to 52.9 fold, Fig. 2e.). Nevertheless, 26/27 of the RU27 plasmas retained residual neutralizing activity against rVSV/SARS-CoV-2_{PMS1-1} (Fig. 2e, Extended Data Fig. 6b). We conclude that some neutralizing epitopes are shared among the convalescent antibodies in high-titer plasmas, but neutralizing activity against SARS-CoV-2 is clearly polyclonal and heterogeneous among individuals with respect to epitope targets.

Polymutant and variant neutralization

We generated a panel of HIV-1 pseudotypes bearing the PMS1-1 spike protein, a second PMS protein with a different set of 13 mutations (selected based on similar criteria, PMSD4), or naturally occurring variants or relatives of SARS-CoV-2 spike (Extended Data Fig. 7a,b) The panel included several SARS-CoV-2 VOC or VOI spike proteins, and spike proteins from sarbecoviruses found in bats (bCoV-RaTG13), pangolins (pCoV-GD and pCoV-GX), and previously in humans (SARS-CoV), that exhibit varying degrees of sequence divergence from SARS-CoV-2²³⁻²⁵ (see Extended Data Fig. 1 for pseudotype characterization). To determine sensitivity/resistance to polyclonal SARS-CoV-2 antibodies, we employed an independent set of 21 randomly selected (Ran1-21) convalescent plasmas, and a set of 14 plasmas from mRNA vaccine recipients (Vac1-14), in addition to the RU27 high-titer plasma panel. The PMS spike proteins exhibited a degree of neutralization resistance that fell with the range of that exhibited by the four SARS-CoV-2 VOC/VOI and the four other sarbecoviruses (Extended Data Fig. 8a-c and 9a-c). Specifically, PMS1-1 and PMSD4 exhibited neutralization resistance that was greater than B.1.1.7 and B.1.526, similar to P.1 and less than B.1.351.3. PMS1-1 and PMSD4 were more resistant to neutralization than pCoV-GD and bCoV-RaTG13, both of which contain a larger number of changes relative to SARS-CoV-2 than the PMS spike proteins. Conversely, the pCoV-GX and SARS-CoV pseudotypes were more resistant to SARS-CoV-2 convalescent or vaccine recipient plasma than PMS1-1 and PMSD4 (Extended Data Fig. 8a-c and 9a-c). Notably, like PMS1-1 and PMSD4, the B.1.351.3 VOC that encodes only nine spike mutations relative to SARS-CoV-2 Wuhan-hu-1, was more neutralization resistant than sarbecoviruses (pCoV-GD and bCoV-RaTG13) that contain a greater number of substitutions, suggesting that the B.1.351.3 mutations were selected by antibody pressure.

A neutralization-resistant polymutant

Based on the above findings, we attempted to generate a mutant SARS-CoV-2 spike protein that was minimally divergent from SARS-CoV-2 Wuhan-hu-1, yet resistant to neutralization by polyclonal convalescent and vaccine recipient plasma. Successful derivation of such a spike protein would identify a complete list of neutralization epitopes recognized by polyclonal antibodies. We chose 20 naturally occurring mutations, including 8 NTD and 8 RBD changes (Fig. 3a) that either (i) arose in our plasma selection experiments (Fig. 2b), (ii) occur in VOC with reduced neutralization sensitivity (Extended Data Fig. 7, 8) or (iii) arose in our previous studies where human monoclonal antibody resistance was selected^{1,2,9}. Naturally occurring deletion mutations in the NTD (Extended Data Fig. 7b), as well as multiple substitutions conferring resistance to class 1, 2, and 3 RBD-binding antibodies^{1,2,9} were included. An rVSV/SARS-CoV-2 derivative encoding the resulting spike sequence, termed PMS20 (Fig. 3a) was replication competent but attenuated compared to rVSV/SARS-CoV-2_{2E1}, suggesting that the 20 mutations confer a fitness cost (Fig 3b). Nevertheless, HIV-1 pseudotypes bearing PMS20, were similarly infectious to those bearing the parental spike protein (Extended Data Fig. 1) and were highly resistant to neutralization.

Indeed, 17/21 random convalescent and 8/14 mRNA vaccinee plasmas gave undetectable neutralization of PMS20 pseudotypes (<1:50, Fig 3c). Among the high-titer convalescent RU27 plasmas 23/27 had residual neutralizing activity against PMS20 that was reduced by a median of 32-fold compared to the parental pseudotype (range 2.8 – 114 fold, Extended Data Fig. 9a). We conclude that the 20 mutations in the PMS20 spike protein are sufficient for evasion of the majority of the antibodies in the plasma of individuals who have been infected by or vaccinated against SARS-CoV-2.

Polyclonal neutralization breadth

In contrast to plasmas from individuals who had been infected or vaccinated, a panel of plasmas from 14 individuals, termed “infected-then-vaccinated” (ITV), who had been both infected by SARS-CoV-2 and subsequently received mRNA vaccines³ retained neutralizing activity against HIV-1 pseudotypes bearing the PMS20 spike (Fig 4a, b). Indeed, the PMS20 mutations that reduced Ran21 and Vac14 plasma NT₅₀ values by a median of 50-fold (range 5.9 to 225 fold) and 81-fold (range 8.4 to 229-fold), respectively, caused a median NT₅₀ reduction of only 18.6-fold (range 3.9 to 100-fold) for the ITV plasma panel (Fig 4a, b). Analysis of chimeric SARS-CoV-2/PMS20 spike proteins in which the respective RBDs were exchanged [PMS20(2-RBD) and SARS-CoV-2(PMS-RBD)] indicated that the relative resistance of the PMS20 to both Ran and ITV plasmas was conferred by multiple spike determinants and that the neutralization breadth in the ITV plasmas was due to antibodies directed at both RBD and non-RBD determinants (Fig. 4a). In addition to the previously reported potent neutralizing activity of ITV plasmas against the B.1.1.7, B.1.525, P.1 and B.1.351.3 VOCs³, the ITV plasmas also potently neutralized B.1.617.2 (delta), as well as a recently described variant (A.VOI.V2)²⁶ that has 11 substitutions and 3 deletions in spike, including an extensively mutated NTD, and is predicted to be resistant to both class 2 and class 3 RBD-binding neutralizing antibodies (Extended Data Fig. 10a).

Plasma from the ITV individuals also had substantial neutralizing activity against heterologous sarbecovirus HIV-1 pseudotypes, including those that were poorly neutralized by Ran21, Vac14 and RU27 plasma panels and whose RBD and/or NTD sequences are extensively divergent from SARS-CoV-2 (Fig 4c, Extended Data Fig. 10a,b). The median NT₅₀ values for the ITV plasmas against sarbecovirus pseudotypes were 5330 (range 2369-7222) for bCoV RaTG13; 3617 (range 1780-6968) for pCoV-GX; 2605 (range 1386-3181) for bCoV-WIV16 and 1208 (range 621-2705) SARS-CoV (Fig. 4c, Extended Data Fig. 10a). Notably, the neutralizing activity of the ITV plasmas against the divergent sarbecoviruses bCoV-WIV16 and SARS-CoV was similar to that found in the random convalescent plasmas against SARS-CoV-2 Wuhan-hu-1. Thus, the neutralization potency and breadth of polyclonal plasma following mRNA vaccination of previously SARS-CoV-2 infected individuals appears greater than previously appreciated.

Discussion

These results indicate the presence of abundant neutralizing antibody targets on the SARS-CoV-2 spike protein. Our recent analyses further suggest that affinity maturation, over months of convalescence, confers antibody flexibility and affinity^{2,3,27} and can impose a requirement for multiple viral substitutions for escape from individual neutralizing antibodies. Some human monoclonal antibodies thus have substantial activity against SARS-CoV-2 variants and divergent sarbecoviruses^{2,28}. Overall, the diversity, maturity and high concentration of neutralizing antibodies likely explains why polyclonal plasma from individuals who have been both infected and subsequently vaccinated could effectively neutralize the otherwise highly neutralization resistant PMS20 polymutant, as well as sarbecoviruses that are divergent from SARS-CoV-2. While standard mRNA vaccine regimens may be less

effective than infection at eliciting individual antibody breadth²⁹, it remains to be seen whether polyclonal neutralization potency and breadth can be achieved using appropriately timed boosting with existing SARS-CoV-2 vaccines. If so, existing immunogens may provide robust protection against future SARS-CoV-2 variants, and a degree of protection against diverse potential future sarbecovirus threats. Conversely, PMS proteins encoding numerous neutralization escape mutations may represent useful immunogens to broaden the polyclonal antibody response elicited by first generation SARS-CoV-2 vaccines.

Online content

Any methods, additional references, Nature Research reporting summaries, source data, extended data, supplementary information, acknowledgements, peer review information; details of author contributions and competing interests; and statements of data and code availability are available at <https://doi.org/10.1038/s41586-021-04005-0>.

1. Weisblum, Y. et al. Escape from neutralizing antibodies by SARS-CoV-2 spike protein variants. *eLife* **9**, e61312, <https://doi.org/10.7554/eLife.61312> (2020).
2. Muecksch, F. et al. Affinity maturation of SARS-CoV-2 neutralizing antibodies confers potency, breadth, and resilience to viral escape mutations. *Immunity*, <https://doi.org/10.1016/j.immuni.2021.07.008> (2021).
3. Wang, Z. et al. Naturally enhanced neutralizing breadth against SARS-CoV-2 one year after infection. *Nature* **595**, 426–431, <https://doi.org/10.1038/s41586-021-03696-9> (2021).
4. Sauer, M. M. et al. Structural basis for broad coronavirus neutralization. *Nature structural & molecular biology*, Online ahead of print, <https://doi.org/10.1038/s41594-021-00596-4> (2021).
5. Schmidt, F. et al. Measuring SARS-CoV-2 neutralizing antibody activity using pseudotyped and chimeric viruses. *The Journal of experimental medicine* **217**, e20201181, <https://doi.org/10.1084/jem.20201181> (2020).
6. Greaney, A. J. et al. Comprehensive mapping of mutations in the SARS-CoV-2 receptor-binding domain that affect recognition by polyclonal human plasma antibodies. *Cell host & microbe* **29**, 463–476, <https://doi.org/10.1016/j.chom.2021.02.003> (2021).
7. Robbiani, D. F. et al. Convergent Antibody Responses to SARS-CoV-2 Infection in Convalescent Individuals. *Nature* **584**, 437–442 (2020).
8. Rogers, T. F. et al. Isolation of potent SARS-CoV-2 neutralizing antibodies and protection from disease in a small animal model. *Science (New York, N.Y.)* **369**, 956–963 (2020).
9. Wang, Z. et al. mRNA vaccine-elicited antibodies to SARS-CoV-2 and circulating variants. *Nature* **592**, 616–622, <https://doi.org/10.1038/s41586-021-03324-6> (2021).
10. Liu, L. et al. Potent neutralizing antibodies against multiple epitopes on SARS-CoV-2 spike. *Nature* **584**, 450–456, <https://doi.org/10.1038/s41586-020-2571-7> (2020).
11. Cao, Y. et al. Potent neutralizing antibodies against SARS-CoV-2 identified by high-throughput single-cell sequencing of convalescent patients' B cells. *Cell* **182**, 1–12, <https://doi.org/10.1016/j.cell.2020.05.025> (2020).
12. McCallum, M. et al. N-terminal domain antigenic mapping reveals a site of vulnerability for SARS-CoV-2. *Cell* **184**, 2332–2347.e2316, <https://doi.org/10.1016/j.cell.2021.03.028> (2021).
13. Cerutti, G. et al. Potent SARS-CoV-2 neutralizing antibodies directed against spike N-terminal domain target a single supersite. *Cell host & microbe* **29**, 819–833.e817, <https://doi.org/10.1016/j.chom.2021.03.005> (2021).
14. Fujino, T. et al. Novel SARS-CoV-2 Variant Identified in Travelers from Brazil to Japan. *Emerging infectious diseases* **27**, 1243–1245, <https://doi.org/10.3201/eid2704.210138> (2021).
15. Volz, E. et al. Assessing transmissibility of SARS-CoV-2 lineage B.1.1.7 in England. *Nature* **593**, 266–269, <https://doi.org/10.1038/s41586-021-03470-x> (2021).
16. Tegally, H. et al. Detection of a SARS-CoV-2 variant of concern in South Africa. *Nature* **592**, 438–443, <https://doi.org/10.1038/s41586-021-03402-9> (2021).
17. West, A. P. et al. Detection and characterization of the SARS-CoV-2 lineage B.1.526 in New York. *bioRxiv : the preprint server for biology*, <https://doi.org/10.1101/2021.02.14.431043> (2021).
18. Wibmer, C. K. et al. SARS-CoV-2 501Y.V2 escapes neutralization by South African COVID-19 donor plasma. *Nature medicine* **27**, 622–625, <https://doi.org/10.1038/s41591-021-01285-x> (2021).
19. Tada, T. et al. Decreased neutralization of SARS-CoV-2 global variants by therapeutic anti-spike protein monoclonal antibodies. *bioRxiv : the preprint server for biology*, <https://doi.org/10.1101/2021.02.18.431897> (2021).
20. Andreano, E. et al. SARS-CoV-2 escape in vitro from a highly neutralizing COVID-19 convalescent plasma. *bioRxiv : the preprint server for biology*, <https://doi.org/10.1101/2020.12.28.424451> (2020).
21. Robbiani, D. F. et al. Recurrent Potent Human Neutralizing Antibodies to Zika Virus in Brazil and Mexico. *Cell* **169**, 597–609.e511, <https://doi.org/10.1016/j.cell.2017.04.024> (2017).
22. Barnes, C. O. et al. Structures of Human Antibodies Bound to SARS-CoV-2 Spike Reveal Common Epitopes and Recurrent Features of Antibodies. *Cell* **182**, 828–842.e816, <https://doi.org/10.1016/j.cell.2020.06.025> (2020).
23. Zhou, P. et al. A pneumonia outbreak associated with a new coronavirus of probable bat origin. *Nature* **579**, 270–273, <https://doi.org/10.1038/s41586-020-2012-7> (2020).

24. Lam, T. T. et al. Identifying SARS-CoV-2-related coronaviruses in Malayan pangolins. *Nature* **583**, 282-285, <https://doi.org/10.1038/s41586-020-2169-0> (2020).
25. Zhang, T., Wu, Q. & Zhang, Z. Probable Pangolin Origin of SARS-CoV-2 Associated with the COVID-19 Outbreak. *Current biology : CB* **30**, 1346-1351.e1342, <https://doi.org/10.1016/j.cub.2020.03.022> (2020).
26. de Oliveira, T. et al. A novel variant of interest of SARS-CoV-2 with multiple spike mutations detected through travel surveillance in Africa. *medRxiv* (2021).
27. Gaebler, C. et al. Evolution of antibody immunity to SARS-CoV-2. *Nature* **591**, 639-644, <https://doi.org/10.1038/s41586-021-03207-w> (2021).
28. Tortorici, M. A. et al. Broad sarbecovirus neutralization by a human monoclonal antibody. *Nature*, <https://doi.org/10.1038/s41586-021-03817-4> (2021).
29. Cho, A. et al. Antibody Evolution after SARS-CoV-2 mRNA Vaccination. *bioRxiv : the preprint server for biology* (2021).

Publisher's note Springer Nature remains neutral with regard to jurisdictional claims in published maps and institutional affiliations.

© The Author(s), under exclusive licence to Springer Nature Limited 2021

ACCELERATED ARTICLE PREVIEW

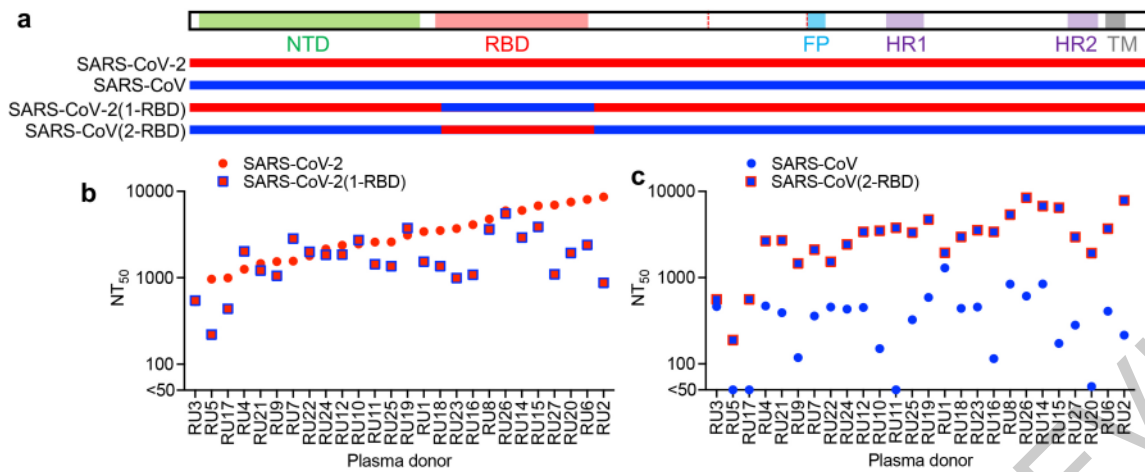


Fig. 1 | Neutralizing antibodies in SARS-CoV-2 convalescent plasma targeting both RBD and non-RBD determinants. (a) Design of RBD-exchanged chimeric spike proteins. **(b,c)** Fifty percent neutralization

titers (NT₅₀) for 26 high titer convalescent plasmas (from the RU1-27 panel) against pseudotyped HIV-1 virions bearing the indicated spike proteins. Median of two independent experiments is plotted.

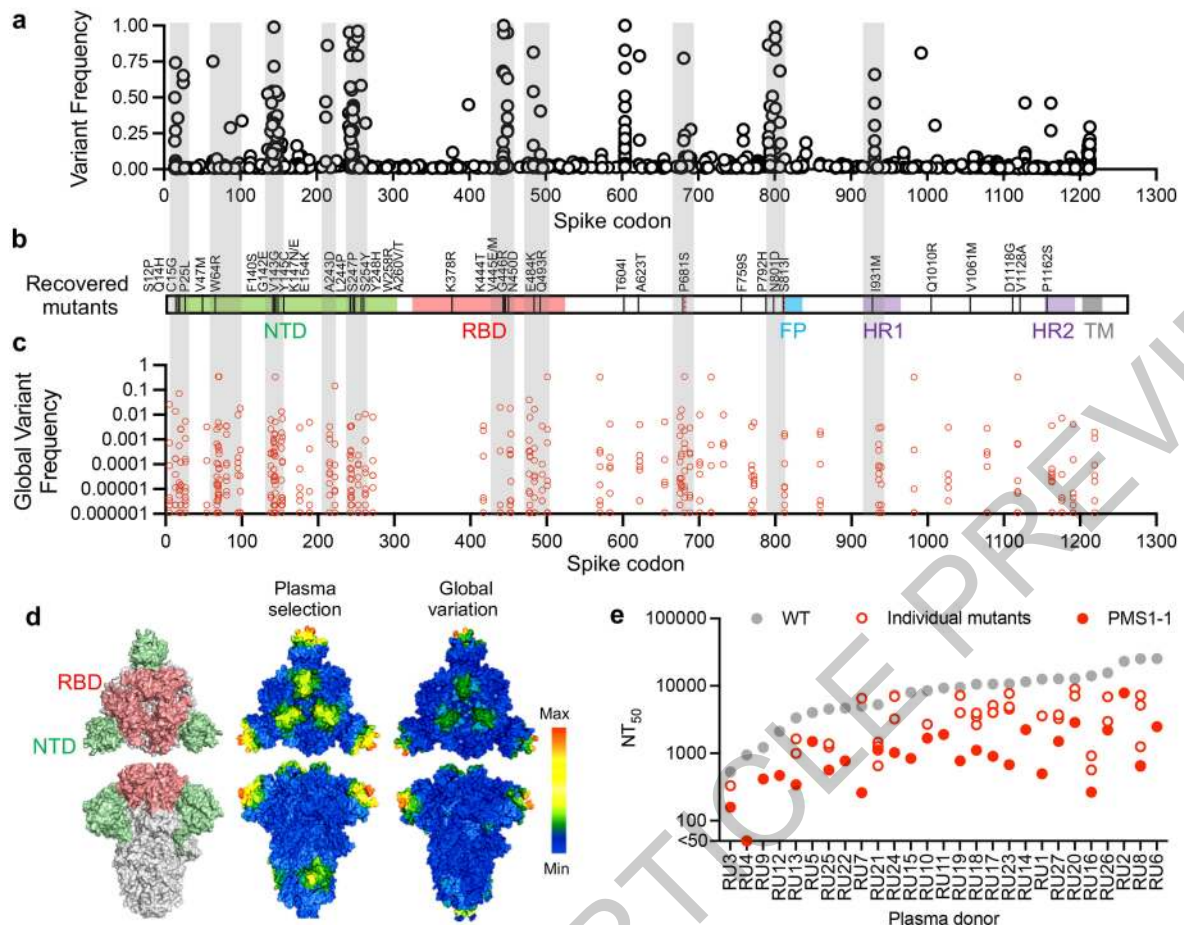


Fig. 2 | Selection of SARS-CoV-2 spike mutants by polyclonal antibodies.

(a) Frequencies of amino acid substitutions at each codon of the SARS-CoV-2 spike protein in two independent rVSV-SARS-CoV-2 populations (1D7 and 2E1), determined by Illumina sequencing. Pooled results following selection with the RU27 plasma panel are displayed. (b) Locations of amino acid substitutions in 38 plaque purified rVSV/SARS-CoV-2 isolates obtained from rVSV/SARS-CoV-2 populations following passage in the RU27 plasmas. (c) Frequencies of naturally occurring amino acid substitutions (red circles) at each codon of the SARS-CoV-2 spike protein. Shaded gray bars in (a-c) indicate shared regions where variation is enriched. (d) Comparison of the averaged

frequency of substitutions observed after passing rVSV/SARS-CoV-2 with RU27 plasmas (center) and the frequency of sequence changes in natural populations (right), projected onto the SARS-CoV-2 spike structure (PDB 6VXX) with positions of the RBD and NTD domains indicated (left). The average frequency of substitutions in a 15 Å radius is represented using the color spectrum (scale = 0-20 center and 0-9 right). (e) Neutralization potency of RU27 plasmas against rVSV/SARS-CoV-2 encoding WT, individual selected mutants, or PMS1-1 spike proteins. Median of two independent determinations is plotted.

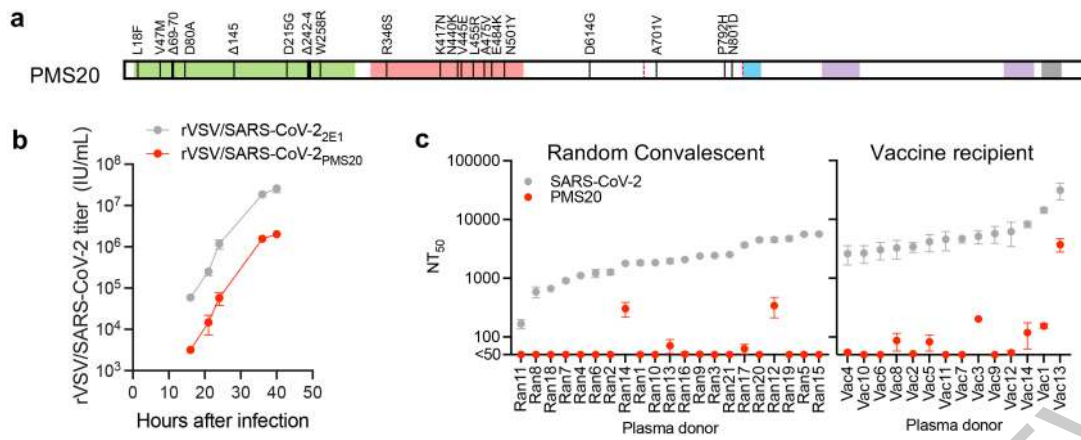


Fig. 3 | Neutralization resistance of polymutant SARS-CoV-2 spike proteins.

(a) Design of the PMS20 spike protein with 20 antibody-selected and VOC-associated mutations. (b) Replication of rVSV/SARS-CoV-2 chimeras encoding 2E1 (parental) or PMS20 spike proteins in 293T/ACE2cl.22 cells infected at a multiplicity of 0.001 and 0.008 respectively. (c) Comparative

neutralization potency of randomly selected convalescent (Ran1-21) and vaccine recipient (Vac1-14) plasmas, against Wuhan-hu-1 and PMS20 (b) SARS-CoV-2 HIV-1 pseudotypes. For b, and c the median \pm range of two independent determinations is plotted.

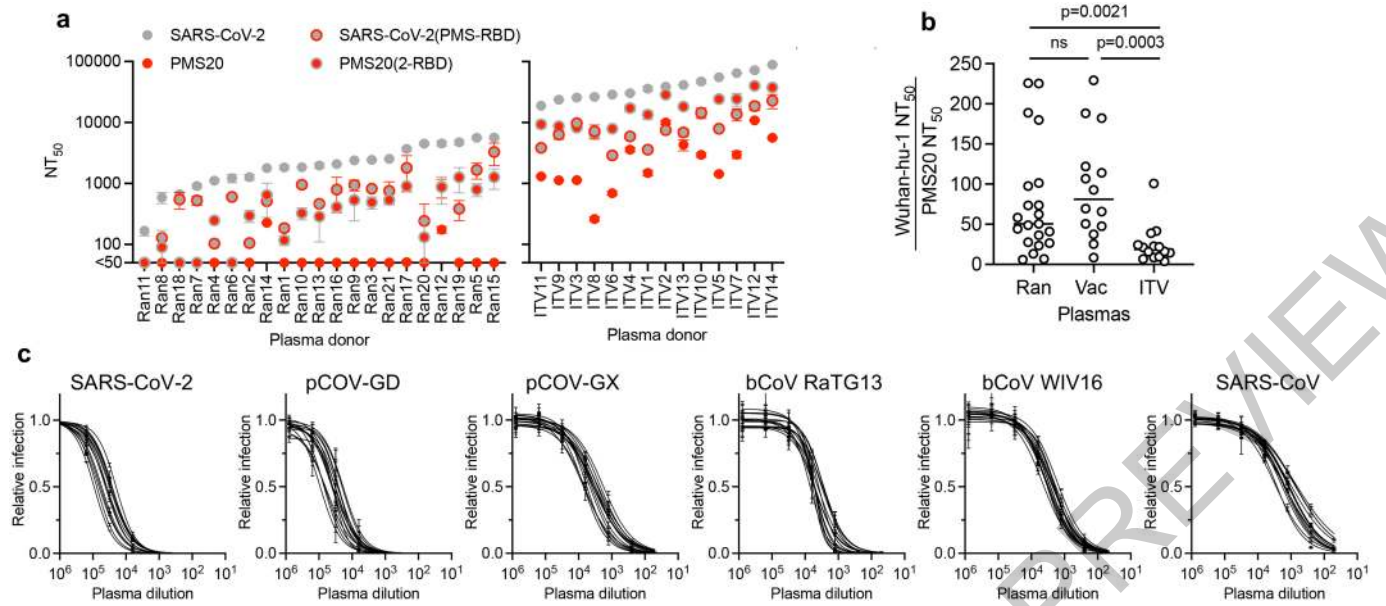


Fig. 4 | Neutralization breadth of polyclonal antibodies from infected-then-vaccinated individuals. (a) Comparative neutralization potency (NT₅₀ values) of random convalescent (Ran1-21) and infected-then-vaccinated (ITV1-14) plasmas against HIV-1 pseudotypes bearing SARS-CoV-2, PMS20, and RBD-exchanged chimeric spike proteins. (b) Fold

difference in NT₅₀, comparing neutralization of HIV-1 pseudotypes bearing SARS-CoV-2 and PMS20 spike proteins by Ran1-21, Vac1-15 and ITV1-14 plasmas (p-values calculated using 2-sided Mann Whitney test). (c) Neutralization curves for ITV plasmas and the indicated sarbecovirus HIV-1 pseudotypes. For (a) and (c) median ± range of two independent determinations is plotted.

Methods

Cell Lines

293T (ATCC CRL-11268), 293T/ACE2cl.22, and HT1080/ACE2.cl.14 cells⁵ were derived from original stocks purchased from the ATCC and were assumed to be authenticated by ATCC. Cells were periodically checked for mycoplasma and retrovirus contamination by DAPI staining and reverse transcriptase assays, respectively.

SARS-CoV-2 and sarbecovirus spike protein pseudotyped reporter viruses

Plasmids pSARS-CoV-2- Δ 19 and pSARS-CoV-2- Δ 19 expressing C-terminally truncated SARS-CoV-2 (NC_045512) and SARS-CoV spike proteins have been described previously⁵ and were used to construct the SARS-CoV-2(1-RBD) and SARS-CoV(2-RBD) expression plasmids in which RBD-encoding sequences were reciprocally exchanged. A panel of plasmids expressing spike proteins from SARS-CoV-2 VOC and VOI were constructed in the context of pSARS-CoV-2- Δ 19 (R683G)⁵. Substitutions were introduced using synthetic gene fragments (IDT) or overlap extension PCR mediated mutagenesis and Gibson assembly. All VOC/VOI and polymutant spike proteins also included the R683G substitution, which disrupts the furin cleavage site and generates higher titer virus stocks without significant effects on pseudotyped virus neutralization sensitivity (Extended Data Fig. 1c, d). The potencies with which the plasma neutralized members of the mutant pseudotype panel were compared with potencies against a “wildtype” SARS-CoV-2 spike sequence, carrying R683G where appropriate. Plasmids expressing the spike proteins found in the horseshoe bat (*Rinolophus affinis*) coronavirus bCoV-RaTG13²³ as well as the pangolin (*Manis javanica*) coronaviruses from Guandong, China (pCoV-GD) and Guanxi, China (pCoV-GX)^{24,25} were similarly constructed. Spike sequences were codon-modified to maximize homology with the human codon-usage optimized of the pSARS-CoV-2 expressing plasmid VG40589-UT (Sinobiological). The 19aa truncated CDS of bCoV-RaTG13 (QHR63300), pCoV-GD (CoV_EPI_ISL_410721), and pCoV-GX (CoV_EPI_ISL_410542) were synthesized by GeneART and subcloned into pCR3.1 using NheI and XbaI and Gibson assembly, and referred to as pCR3.1-bCoV-RaTG13- Δ 19, pCR3.1pCoV-GD- Δ 19 and pCR3.1pCoV-GX- Δ 19, respectively. Pseudotyped HIV-1 particles were generated as previously described⁵. Specifically, virus stocks were harvested 48 hours after transfection of 293T cells with pHIV-1 GagPol and pCCNano/LucGFP (Fig.1) or pNL4-3 Δ Env-nanoluc (all other Figs) along with a spike expression plasmid, filtered and stored at -80°C.

SARS-CoV-2/sarbecovirus pseudotype neutralization assays

Plasmas were five-fold serially diluted and then incubated with pseudotyped HIV-1 reporter virus for 1h at 37°C. The antibody/pseudotype virus mixture was then added to HT1080/ACE2.cl14 cells. After 48 h, cells were washed with PBS, lysed with Luciferase Cell Culture Lysis reagent (Promega) and NanoLuc Luciferase activity in lysates was measured using the Nano-Glo Luciferase Assay System (Promega) and a Glomax Navigator luminometer (Promega). The relative luminescence units were normalized to those derived from cells infected with the pseudotyped virus in the absence of plasma. The half-maximal neutralizing titer (NT₅₀) was determined using four-parameter nonlinear regression (least squares regression method without weighting) (GraphPad Prism).

Plasma samples

Plasma samples were from individuals who were infected with SARS-CoV-2 a mean of 1.3 months prior to plasma donation⁷ or from individuals who had received mRNA vaccines at various times prior to plasma donation⁹. A set of twenty-seven plasma samples from SARS-CoV-2 infected individuals with high neutralizing activity who had not been vaccinated⁷, termed the “RU27” plasma panel were used in VSV-SARS-CoV-2 selection procedures, while this panel plus a second set of 21 randomly selected

plasmas (selected at random with blinding to neutralization titer or any demographic characteristic) from the same convalescent cohort formed the “Ran21” plasma panel⁷. A set of 14 plasmas donated by individuals who had received a Pfizer/BionTech mRNA vaccine formed the “Vac14” plasma panel⁹. Finally a set of 15 plasmas from convalescent individuals who had received a Pfizer/BionTech mRNA vaccine between 6 and 12 months after infection³ formed the infected-then-vaccinated “ITV15” plasma panel. The study visits and blood draws were obtained with informed consent from all participants under a protocol that was reviewed and approved by the Institutional Review Board of the Rockefeller University (IRB no. DRO-1006, ‘Peripheral Blood of Coronavirus Survivors to Identify Virus-Neutralizing Antibodies’).

Selection of antibody resistant rVSV/SARS-CoV-2 variants

To select plasma-resistant spike variants, rVSV/SARS-CoV-2/GFP_{ID7} and rVSV/SARS-CoV-2/GFP_{2E1} were passaged to generate diversity, and populations containing 10⁶ PFU were incubated with plasma (diluted 1:50 to 1:400) for 1h at 37°C before inoculation of 2x10⁵ 293T/ACE2cl.22 cells in 6-well plates. The following day the medium was replaced with fresh medium containing the same concentrations of plasma. Supernatant from the wells containing the highest concentrations of plasma antibodies that showed evidence of rVSV/SARS-CoV-2/GFP replication (large numbers of GFP positive cells or GFP positive foci) was harvested 24h later. Thereafter, aliquots (100 μ l) of the cleared supernatant from the first passage (p1) were incubated with the same or increased concentration of plasma and then used to infect 2x10⁵ 293T/ACE2cl.22 cells in 6-well plates, as before (p2). In situations where small, but expanding GFP-positive foci were observed, the medium was refreshed at 48h with fresh medium containing no plasma and the virus harvested 24h later. We repeated this process for up to 6 passages or until reduced neutralization potency for the plasma was obvious, as indicated by visual detection of increasing numbers of GFP positive cells during passage.

To isolate individual mutant viruses by limiting dilution, the selected rVSV/SARS-CoV-2/GFP_{ID7} and rVSV/SARS-CoV-2/GFP_{2E1} populations were serially diluted in the absence of plasma and aliquots of each dilution added to individual wells of 96-well plates containing 1x10⁴ 293T/ACE2cl.22 cells. Individual viral variants were identified by observing single GFP-positive plaques in individual wells at limiting dilutions. The plaque-purified viruses were expanded, RNA was extracted, and spike sequences determined.

rVSV/SARS-CoV-2 neutralization assays

Plasma samples were five-fold serially diluted and then incubated with rVSV/SARS-CoV-2/GFP_{ID7} and rVSV/SARS-CoV-2/GFP_{2E1}, or plaque purified selected variants thereof, for 1 h at 37°C. The antibody/recombinant virus mixture was then added to 293T/ACE2.cl22 cells. After 16h, cells were harvested, and infected cells were quantified by flow cytometry. The percentage of infected cells was normalized to that derived from cells infected with rVSV/SARS-CoV-2 in the absence of plasma. The half-maximal neutralizing titer for each plasma (NT₅₀) was determined using four-parameter nonlinear regression (least squares regression method without weighting) (GraphPad Prism).

Sequence analyses

To identify putative antibody resistance mutations, RNA was isolated from aliquots of supernatant containing selected viral populations or individual plaque purified variants using NucleoSpin 96 Virus Core Kit (Macherey-Nagel). The purified RNA was subjected to reverse transcription using random hexamer primers and SuperScript VILO cDNA Synthesis Kit (Thermo Fisher Scientific). The cDNA was amplified using KOD Xtreme Hot Start DNA

Polymerase (Millipore Sigma). Specifically, a fragment including the coding region of the extracellular domain of spike was amplified using primers targeting the intergenic region between VSV-M and spike, and the spike intracellular domain. The PCR products were purified and sequenced either using Sanger-sequencing or Illumina sequencing

Article

as previously described³⁰. For Illumina sequencing, 1 µl of diluted DNA was used with 0.25 µl Nextera TDE1 Tagment DNA enzyme (catalog no. 15027865), and 1.25 µl TD Tagment DNA buffer (catalog no. 15027866; Illumina). Then, the DNA was ligated to i5/i7 barcoded primers using the Illumina Nextera XT Index Kit v2 and KAPA HiFi HotStart ReadyMix (2X; KAPA Biosystems). Next the DNA was purified using AmPure Beads XP (Agencourt), pooled, sequenced (paired end) using Illumina MiSeq Nano 300 V2 cycle kits (Illumina) at a concentration of 12pM.

For analysis of the Illumina sequencing data, adapter sequences were removed from the raw reads and low-quality reads (Phred quality score <20) using BBDuk. Filtered reads were mapped to the codon-optimized SARS-CoV-2 S sequence in rVSV/SARS-CoV-2/GFP and mutations were annotated using Geneious Prime (Version 2020.1.2), using a P-value cutoff of 10⁻⁶. RBD-specific variant frequencies, P-values, and read depth were compiled using Python running pandas (1.0.5), numpy (1.18.5), and matplotlib (3.2.2). The parental rVSV/SARS-CoV-2/GFP 2E1 and 1D7 sequences each contain two adaptive mutations (1D7, F157S and R685M for 1D7; D215G and R683G for 2E1) but each was considered “WT” for the purposes of the plasma selection experiments and were subtracted from the analyses of the sequences.

The frequency of amino acid substitutions during rVSV/SARS-CoV-2 passage in plasmas was compared with the frequency of global occurrences of changes at each residue on 5/11/21 (Los Alamos, COVID-19 Viral Genome Analysis Pipeline, <https://cov.lanl.gov/content/index>)³¹. For comparison of SARS-CoV-2 with sarbecoviruses, amino acid sequences were aligned with Clustal Omega. Using a python script clone of Simplot (<https://jonathanrd.com/20-05-02-writing-a-simplot-clone-in-python/>), the percent identity relative to SARS-CoV2 was calculated within a rolling window of 100 amino acids, stepping a single residue at a time.

For three-dimensional sliding window analysis of changes in the spike amino acid sequence observed globally and in vitro, the frequency of global occurrences of changes at each residue (Los Alamos, COVID-19 Viral Genome Analysis Pipeline, <https://cov.lanl.gov/content/index>)³¹ was divided by the average frequency of change at any residue and projected in the SARS-CoV-2 spike structure PDB 6VXX³² as relative change frequency using BioStructMap^{33,34}. Alternatively, the averaged frequency of substitutions observed after passaging rVSV/SARS-CoV-2 with plasma was divided by the mean substitution frequency and applied as a 3D sliding window over the spike structure. The average frequency of substitutions in a 15 Å radius is represented using a color spectrum.

Reporting summary

Further information on research design is available in the Nature Research Reporting Summary linked to this paper.

Data availability

Data are on plasma selected mutations are provided in Supplementary Table 1. Neutralization assay datasets generated during the current study are available in the accompanying supplementary source data files. Source data are provided with this paper.

Code availability

Analyses used commercially available software. No new code was generated

30. Gaebler, C. et al. Combination of quadruplex qPCR and next-generation sequencing for qualitative and quantitative analysis of the HIV-1 latent reservoir. *The Journal of experimental medicine* **216**, 2253-2264, <https://doi.org/10.1084/jem.20190896> (2019).
31. Korber, B. et al. Tracking Changes in SARS-CoV-2 Spike: Evidence that D614G Increases Infectivity of the COVID-19 Virus. *Cell* **182**, 812-827.e819, <https://doi.org/10.1016/j.cell.2020.06.043> (2020).
32. Walls, A. C. et al. Structure, Function, and Antigenicity of the SARS-CoV-2 Spike Glycoprotein. *Cell* **181**, 281-292.e286, <https://doi.org/10.1016/j.cell.2020.02.058> (2020).
33. Guy, A. J., Irani, V., Richards, J. S. & Ramsland, P. A. BioStructMap: a Python tool for integration of protein structure and sequence-based features. *Bioinformatics (Oxford, England)* **34**, 3942-3944, <https://doi.org/10.1093/bioinformatics/bty474> (2018).
34. Guy, A. J. et al. Proteome-wide mapping of immune features onto Plasmodium protein three-dimensional structures. *Scientific reports* **8**, 4355, <https://doi.org/10.1038/s41598-018-22592-3> (2018).

Acknowledgements This work was supported by NIH grants R37AI64003 and R01AI50111 (P.D.B.), R01AI78788 (T.H.), P01-AI138398-S1 (M.C.N.) and 2U19AI111825 (M.C.N.). C.G. was supported by the Robert S. Wennett Post-Doctoral Fellowship, in part by the National Center for Advancing Translational Sciences (National Institutes of Health Clinical and Translational Science Award programme, grant UL1 TR001866), and by the Shapiro-Silverberg Fund for the Advancement of Translational Research. P.D.B. and M.C.N. are Howard Hughes Medical Institute Investigators.

Author contributions P.D.B., T.H., M.C.N., F.S., and Y.W. conceived, designed and analyzed the experiments. F.S., Y.W., constructed and performed rVSV/SARS-CoV-2 selection and neutralization experiments. F.S., Y.W., M.R., J.D.S. and E.B. performed pseudotype neutralization experiments. F.S., T.H. and F.Z. constructed expression plasmids. A.C. performed NGS. D.P. and F.S. performed bioinformatic analysis. M.C., C.G. and D. J. S-B executed clinical protocols and recruited participants and processed samples. P.D.B., T.H., F.S., and Y.W. wrote the manuscript with input from all co-authors.

Competing interests P.D.B. has received remuneration from Pfizer Inc. for consulting on mRNA vaccines.

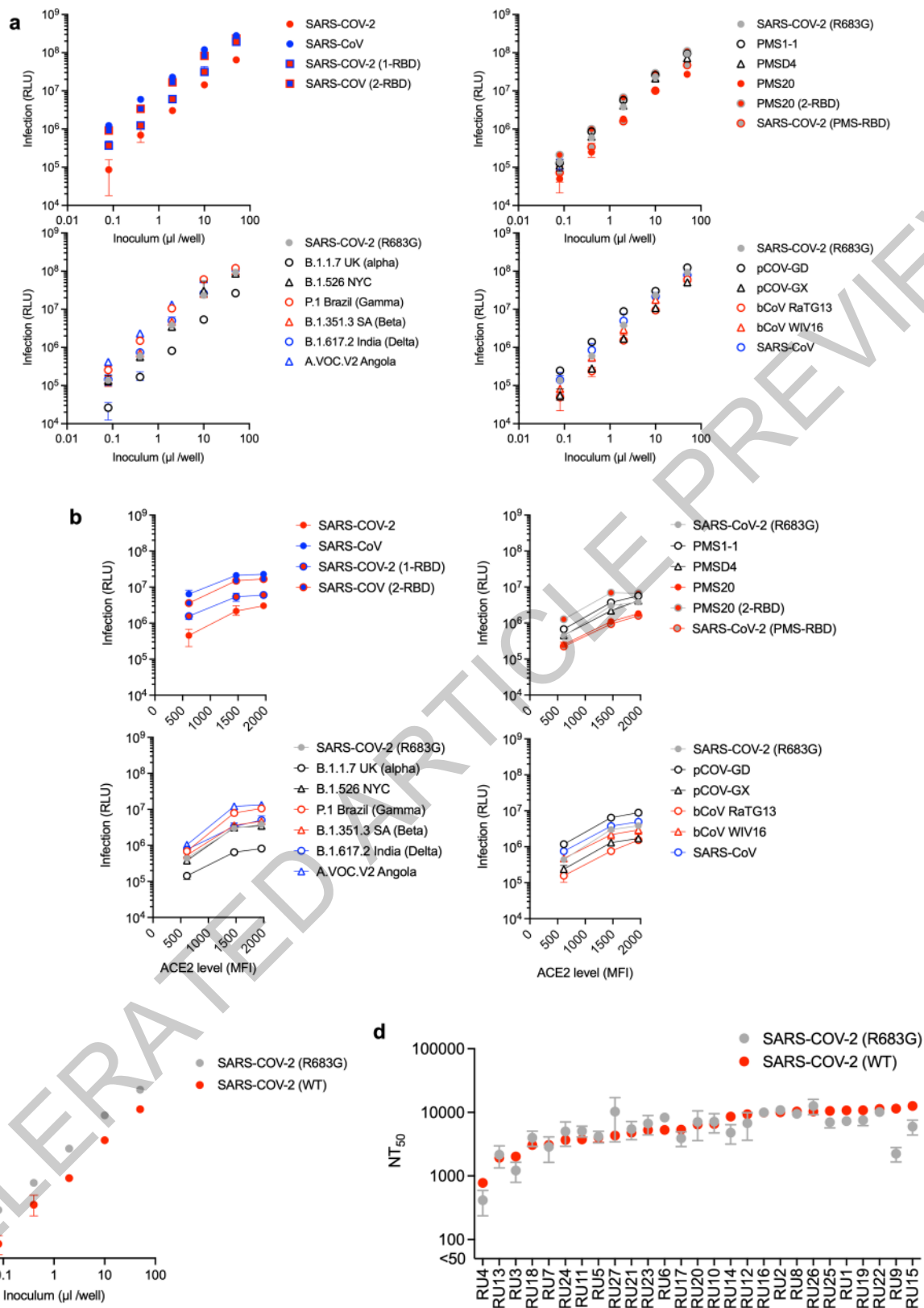
Additional information

Supplementary information The online version contains supplementary material available at <https://doi.org/10.1038/s41586-021-04005-0>.

Correspondence and requests for materials should be addressed to T.H. or P.D.B..

Peer review information Nature thanks the anonymous reviewer(s) for their contribution to the peer review of this work.

Reprints and permissions information is available at <http://www.nature.com/reprints>.



Extended Data Fig. 1 | See next page for caption.

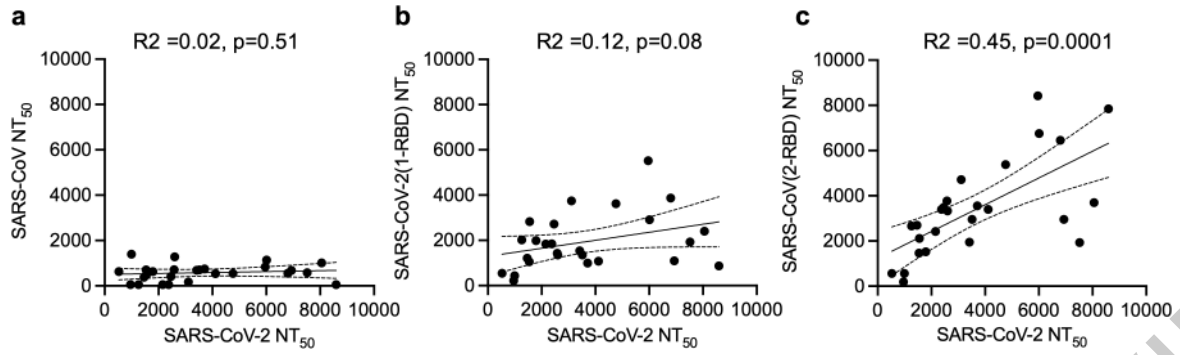
Article

Extended Data Fig. 1 | Characterization of HIV-1 pseudotypes bearing the chimeric, mutant, and variant SARS-CoV-2 and sarbecovirus spike proteins.

(a) Titration of pseudotyped viruses on 293T/ACE2cl.22 cells. Chimeric spike pseudotyped viruses in the upper left panel were built using the unaltered SARS-CoV-2 Δ 19 and SARS-CoV Δ 19 spike protein constructs and a 3-plasmid HIV-1 pseudotyping system (see Methods). The other panels depict titration of pseudotypes derived using a furin cleavage site mutant SARS-CoV-2 Δ 19 spike protein (R683G) and a 2-plasmid HIV-1 pseudotyping system (see Methods). **(b)** The same pseudotyped viruses used in **(a)** were used to

infect 3 different 293T/ACE2 clonal cell lines each expressing a different level of ACE2 (MFI = mean fluorescence intensity). **(c)** Titration of pseudotypes bearing an unaltered SARS-CoV-2 Δ 19 spike protein and a furin cleavage site mutant SARS-CoV-2 Δ 19 spike protein (R683G) generated using a 2-plasmid HIV-1 pseudotype system (see Methods). **(d)** Comparative neutralization potency (NT_{50} values) of high titer convalescent (RU27) plasmas against HIV-1 pseudotypes bearing R683G mutant (grey symbols) and unaltered (red symbols) SARS-CoV-2 Δ 19 spike proteins. For all panels, median \pm range of two independent experiments is plotted.

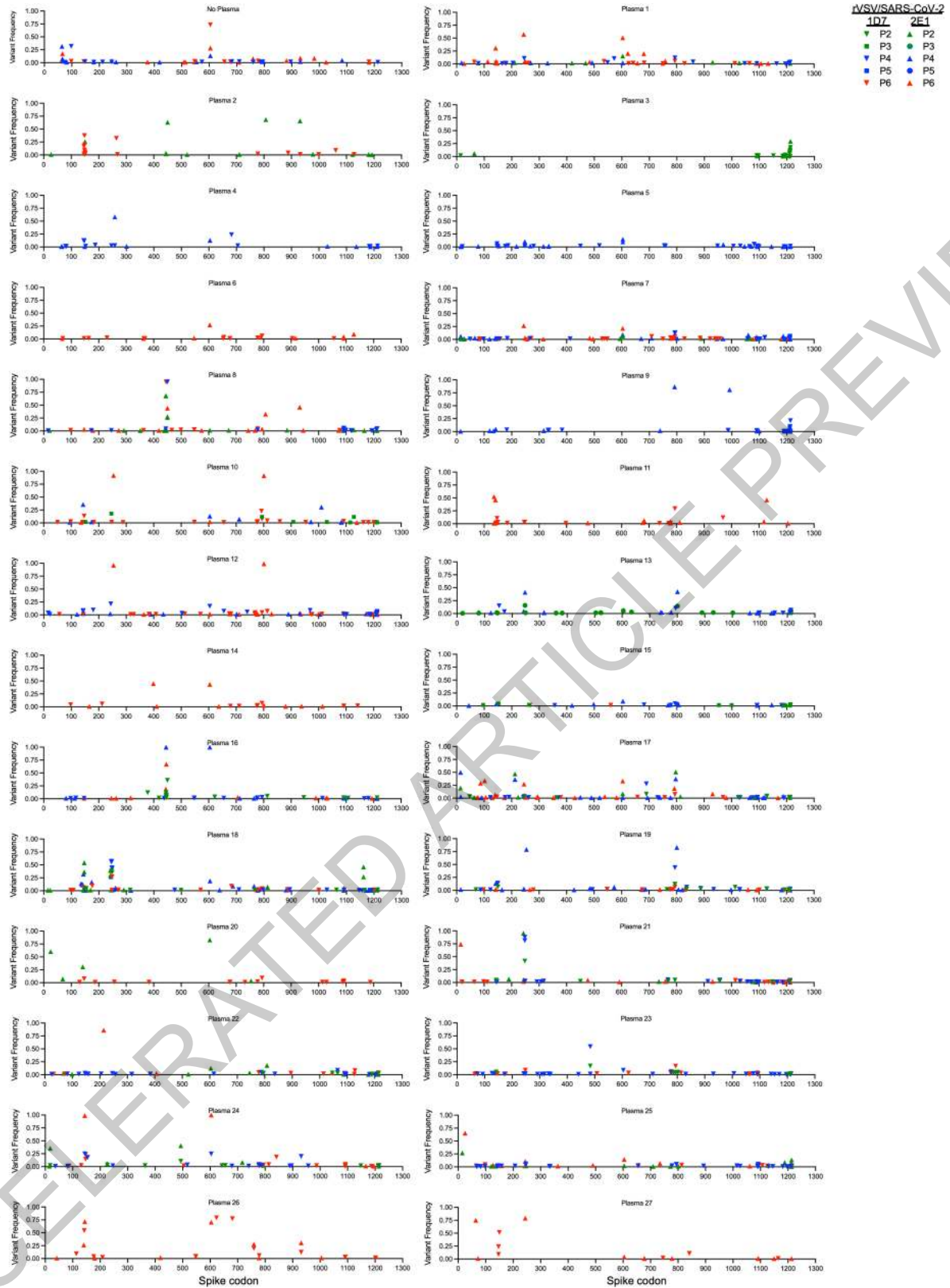
ACCELERATED ARTICLE PREVIEW



Extended Data Fig. 2 | The RU27 SARS-CoV-2 convalescent plasma panel contains neutralizing antibodies targeting RBD and non-RBD determinants. (a-c) Correlations of neutralizing potencies of the RU27

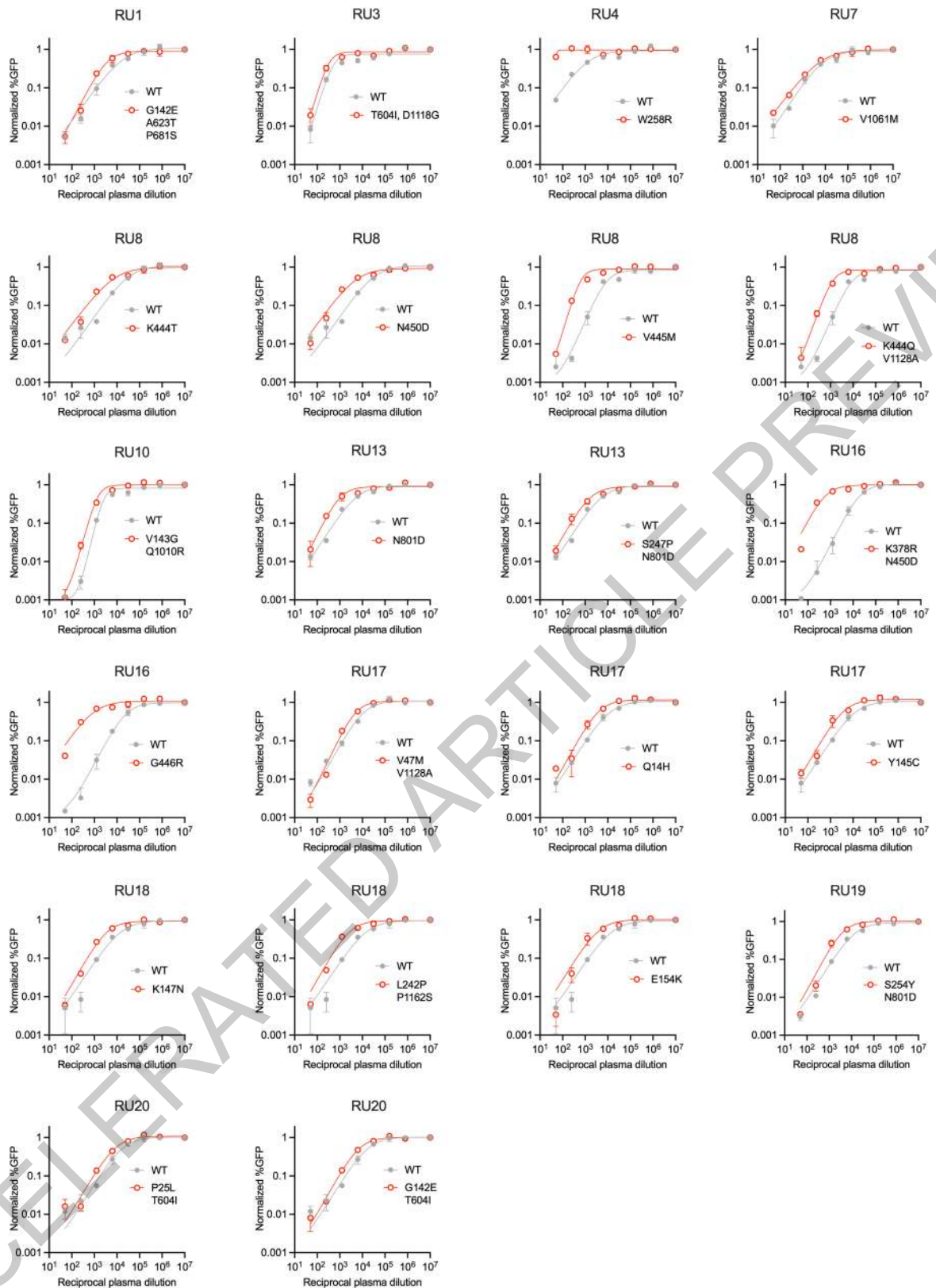
plasmas against psudotypes bearing the indicated pairs of spike proteins. Simple linear regression was used to calculate R2 and p-values, dashed lines indicate 95% confidence intervals for the regression line.

ACCELERATED ARTICLE PREVIEW



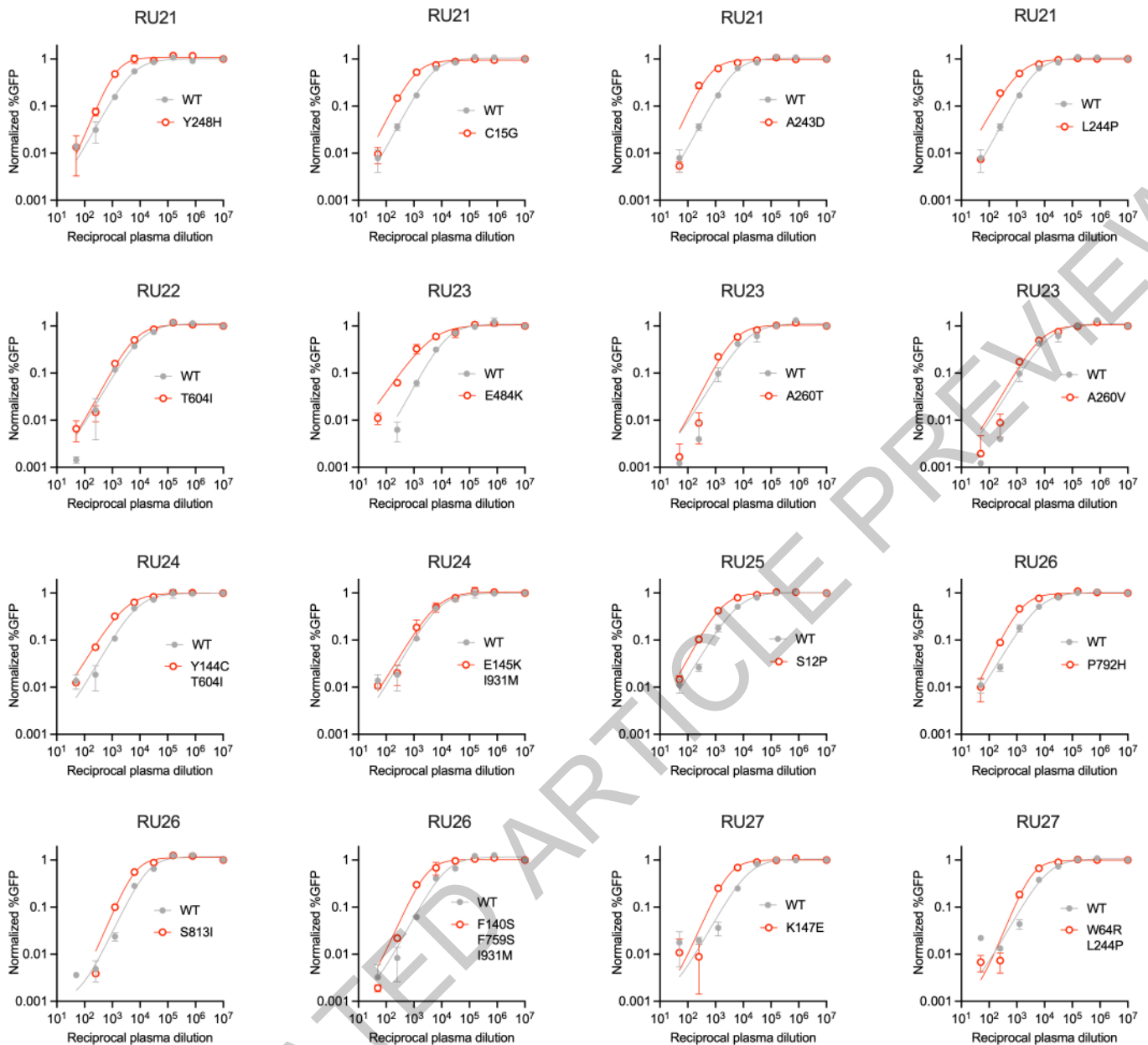
Extended Data Fig. 3 | Selection pressure on SARS-CoV-2 spike exerted by convalescent plasma. Frequencies of amino acid substitutions at each codon of the SARS-CoV-2 spike protein following the indicated number of passages

(P2-P6) of two independent rVSV-SARS-CoV-2 populations (1D7 and 2E1), in each of the RU27 plasmas, determined by NGS sequencing.



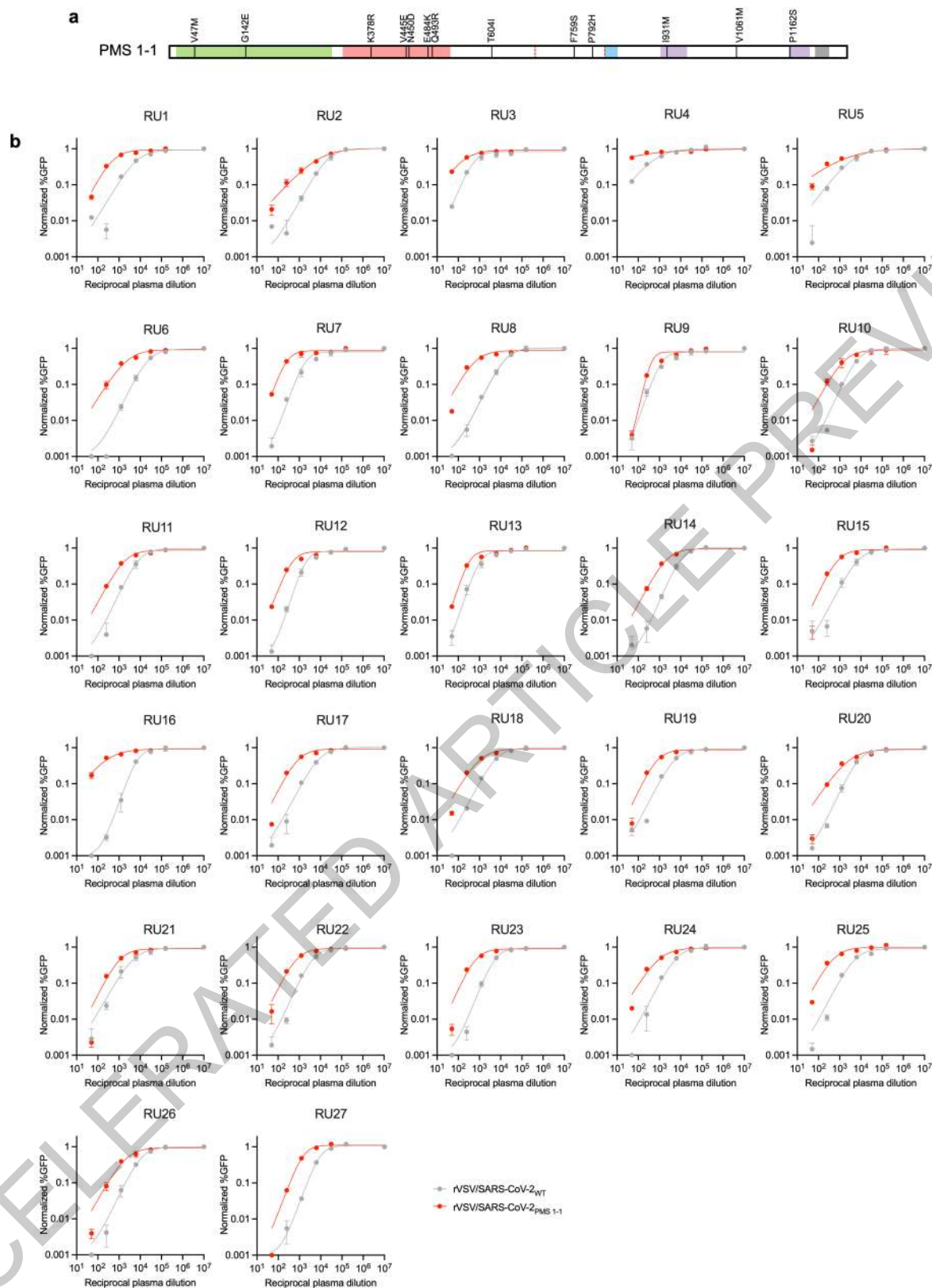
Extended Data Fig. 4 | Neutralization sensitivity of plasma-selected rVSV/SARS-CoV-2 mutants to RU1-20 plasmas. Infection, relative to non-neutralized controls, by plaque purified rVSV/SARS-CoV-2 isolates in the presence of the indicated dilutions of the indicated plasmas from the RU27

panel. The same plasmas that were used to select the indicated mutants were used to determine neutralization potency against the respective plaque purified mutants (red) and parental (WT, grey) rVSV/SARS-CoV-2 1D7 or 2E1 viruses. Median \pm range of two technical replicates is plotted.



Extended Data Fig. 5 | Neutralization sensitivity of plasma-selected rVSV/SARS-CoV-2 mutants to RU21-27 plasmas. Infection, relative to non-neutralized controls, by plaque purified rVSV/SARS-CoV-2 isolates in the presence of the indicated dilutions of the indicated plasmas from the RU27

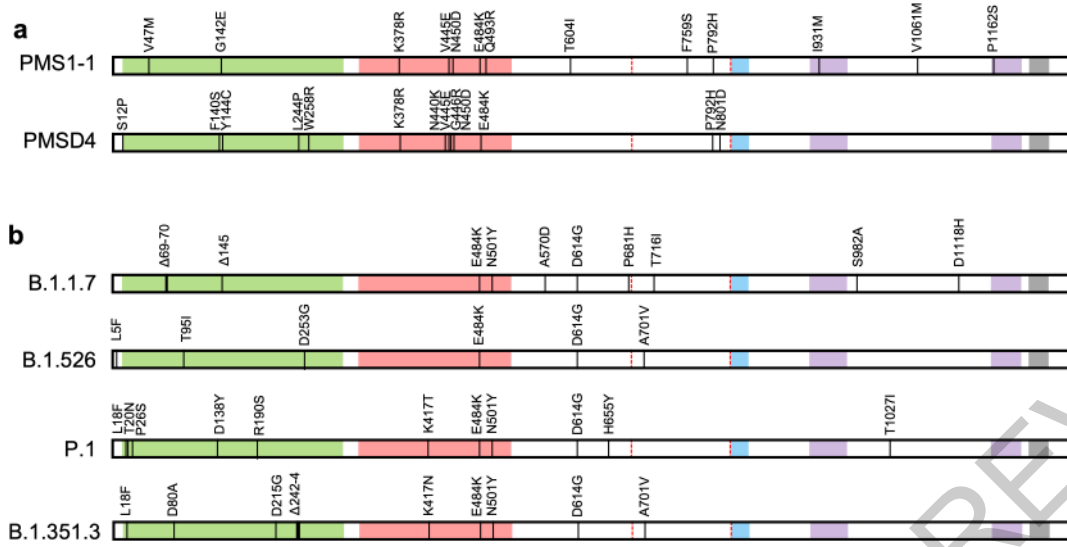
panel. The same plasmas that were used to select the indicated mutants were used to determine neutralization potency against the respective plaque purified mutants (red) and parental (WT, grey) rVSV/SARS-CoV-2 1D7 or 2E1 viruses. Median \pm range of two technical replicates is plotted.



Extended Data Fig. 6 | Neutralization sensitivity of rVSV/SARS-CoV-2 encoding the PMS1-1 spike. (a) Design of the PMS1-1 polymutant spike protein with 13 plasma-selected spike mutations aggregated in a single spike.

(b) Infection, relative to non-neutralized controls, by rVSV/SARS-CoV-2_{PMS1-1}

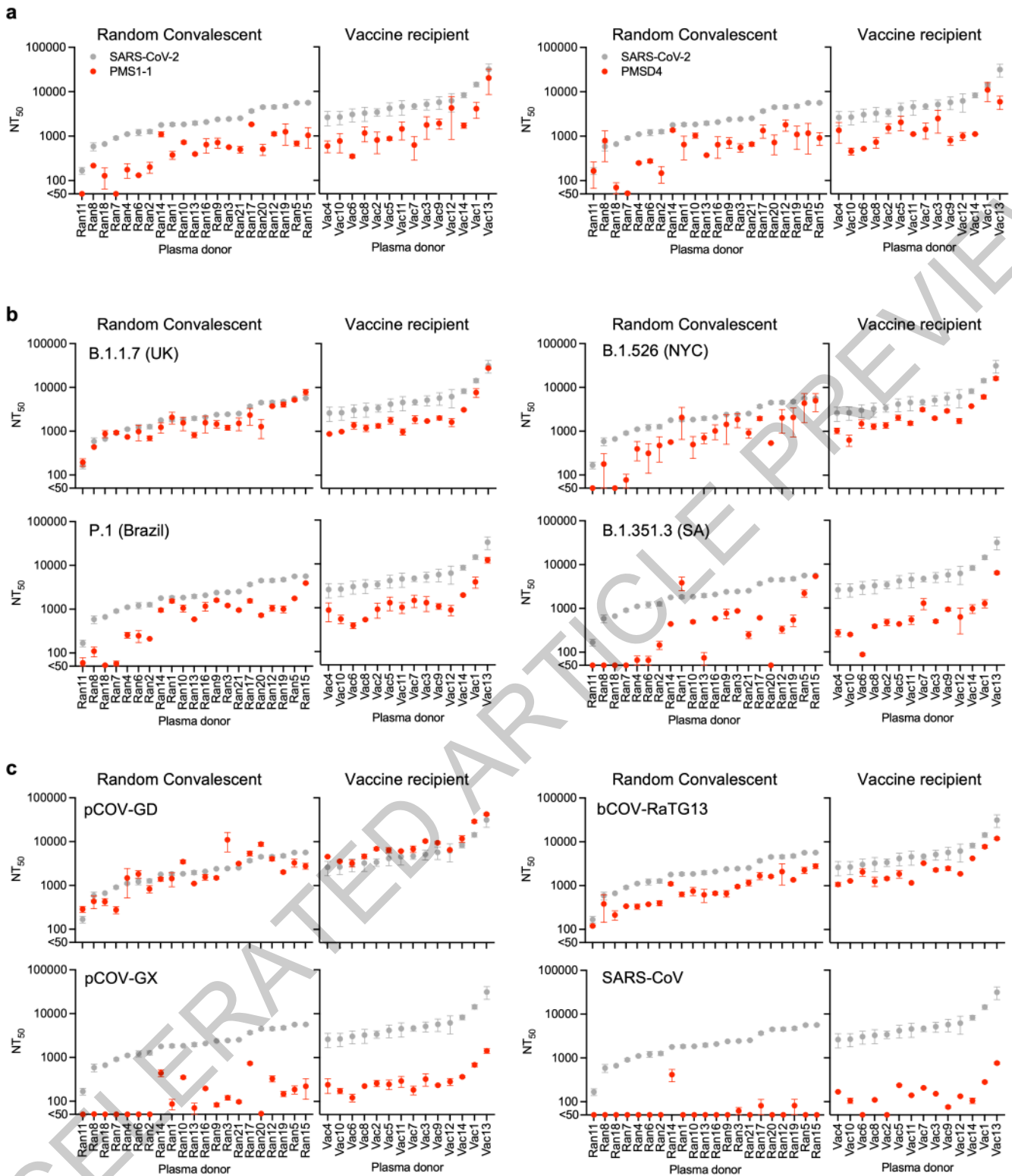
(red) and rVSV/SARS-CoV-2_{2E1} (grey) in the presence on the indicated dilutions of the plasmas from the RU27 panel. Median \pm range of two technical replicates is plotted.



Extended Data Fig. 7 | Synthetic polymutant and natural variant SARS-CoV-2 spike proteins. (a) Design of the PMS1-1 and PMSD4 polymutant spike proteins with 13 plasma-selected spike mutations aggregated in each

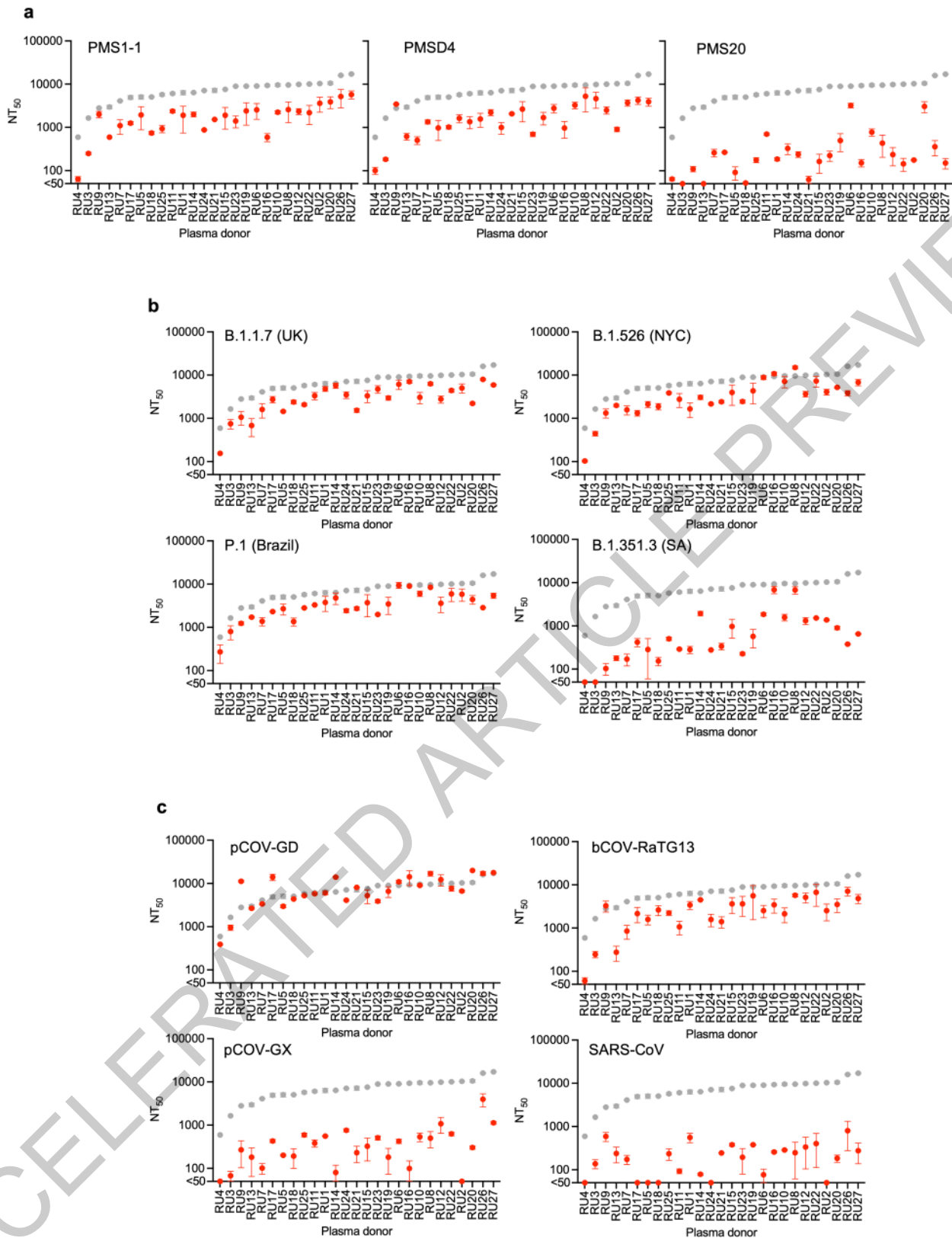
spike. (b) Schematic representation of mutations in naturally occurring VOC/VOI SARS-CoV-2 spike proteins.

ACCELERATED ARTICLE PREVIEW



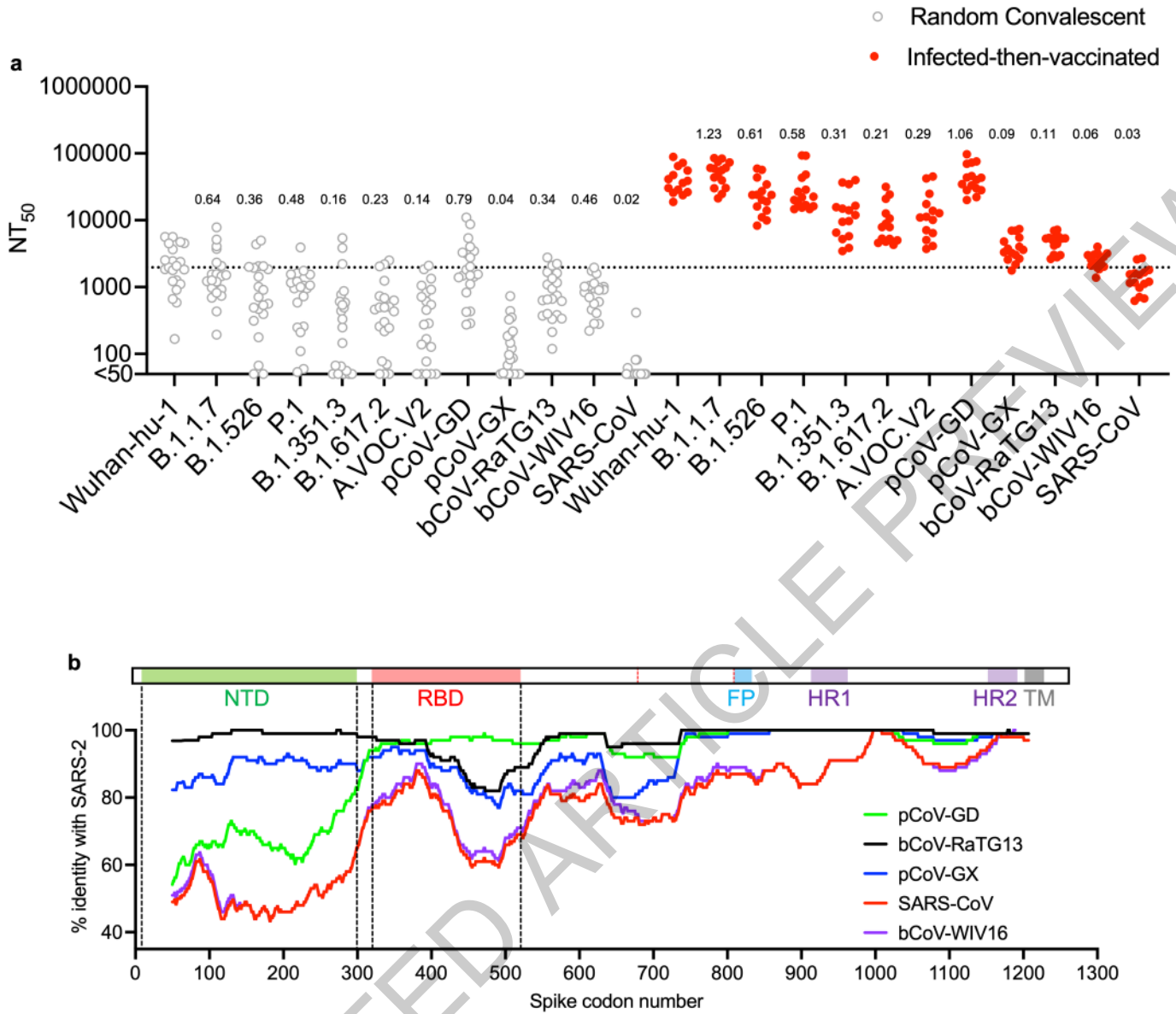
Extended Data Fig. 8 | Neutralization potency of random convalescent and vaccine recipient plasmas against polymutant, VOC/VOI, and sarbecovirus HIV-1 pseudotypes. (a-c) Comparative neutralization potency (NT₅₀ values) of random convalescent (Ran1-21) and vaccine recipient (Vac1-14) plasmas plasma

against WT (grey symbols) and the indicated SARS-CoV-2 synthetic polymutant (a), natural variant (b) or sarbecovirus (c) (red symbol) HIV-1 pseudotypes. For all panels, median \pm range of two independent experiments is plotted.



Extended Data Fig. 9 | Neutralization potency of high titer convalescent plasma against PMS, VOC/VOI, and sarbecovirus HIV-1 pseudotypes.
(a-c) Comparative neutralization potency (NT_{50} values) of high titer convalescent (RU27) plasma against WT (grey symbols) and indicated

polymutant (a), SARS-CoV-2 natural variant (b) or sarbecovirus (c) (red symbol) HIV-1 pseudotypes. For all panels, median \pm range of two independent experiments is plotted.



Extended Data Fig. 10 | Neutralization potency of plasma from infected-then-vaccinated against VOC/VOI and diverse sarbecovirus HIV-1 pseudotypes. (a) Neutralization potency (NT₅₀ values) of random convalescent plasmas (grey symbols) or ITV plasmas (red symbols) against SARS-CoV-2 prototype or variant or sarbecovirus HIV-1 pseudotypes. Median of two independent experiments is plotted. Dashed line indicated median NT₅₀

for random convalescent plasmas against Wuhan-Hu-1 SARS-CoV-2. Numbers above each scatterplot indicate the median NT₅₀ relative to the median NT₅₀ for Wuhan-Hu-1 SARS-CoV-2. (b) Sequence diversity across sarbecovirus spike domains; SARS-CoV-2 and the indicated sarbecovirus spike sequences were aligned with Clustal and compared using Simplot; the percent identity relative to SARS-CoV-2 was plotted within a rolling window of 100 amino acids.

Reporting Summary

Nature Portfolio wishes to improve the reproducibility of the work that we publish. This form provides structure for consistency and transparency in reporting. For further information on Nature Portfolio policies, see our [Editorial Policies](#) and the [Editorial Policy Checklist](#).

Statistics

For all statistical analyses, confirm that the following items are present in the figure legend, table legend, main text, or Methods section.

- | n/a | Confirmed |
|-------------------------------------|---|
| <input type="checkbox"/> | <input checked="" type="checkbox"/> The exact sample size (n) for each experimental group/condition, given as a discrete number and unit of measurement |
| <input type="checkbox"/> | <input checked="" type="checkbox"/> A statement on whether measurements were taken from distinct samples or whether the same sample was measured repeatedly |
| <input type="checkbox"/> | <input checked="" type="checkbox"/> The statistical test(s) used AND whether they are one- or two-sided
<i>Only common tests should be described solely by name; describe more complex techniques in the Methods section.</i> |
| <input checked="" type="checkbox"/> | <input type="checkbox"/> A description of all covariates tested |
| <input checked="" type="checkbox"/> | <input type="checkbox"/> A description of any assumptions or corrections, such as tests of normality and adjustment for multiple comparisons |
| <input checked="" type="checkbox"/> | <input type="checkbox"/> A full description of the statistical parameters including central tendency (e.g. means) or other basic estimates (e.g. regression coefficient) AND variation (e.g. standard deviation) or associated estimates of uncertainty (e.g. confidence intervals) |
| <input checked="" type="checkbox"/> | <input type="checkbox"/> For null hypothesis testing, the test statistic (e.g. F , t , r) with confidence intervals, effect sizes, degrees of freedom and P value noted
<i>Give P values as exact values whenever suitable.</i> |
| <input checked="" type="checkbox"/> | <input type="checkbox"/> For Bayesian analysis, information on the choice of priors and Markov chain Monte Carlo settings |
| <input checked="" type="checkbox"/> | <input type="checkbox"/> For hierarchical and complex designs, identification of the appropriate level for tests and full reporting of outcomes |
| <input checked="" type="checkbox"/> | <input type="checkbox"/> Estimates of effect sizes (e.g. Cohen's d , Pearson's r), indicating how they were calculated |

Our web collection on [statistics for biologists](#) contains articles on many of the points above.

Software and code

Policy information about [availability of computer code](#)

Data collection Attune for FACS analysis of GFP expression. Glowmax Navigator Promega for naniluc assays

Data analysis GraphPad Prism, BBDuk, Geneious Prime (Version 2020.1.2), Python running pandas (1.0.5), numpy (1.18.5), and matplotlib (3.2.2), python script clone of Simplot (<https://jonathanrd.com/20-05-02-writing-a-simplot-clone-in-python/>)

For manuscripts utilizing custom algorithms or software that are central to the research but not yet described in published literature, software must be made available to editors and reviewers. We strongly encourage code deposition in a community repository (e.g. GitHub). See the Nature Portfolio [guidelines for submitting code & software](#) for further information.

Data

Policy information about [availability of data](#)

All manuscripts must include a [data availability statement](#). This statement should provide the following information, where applicable:

- Accession codes, unique identifiers, or web links for publicly available datasets
- A description of any restrictions on data availability
- For clinical datasets or third party data, please ensure that the statement adheres to our [policy](#)

The datasets generated during and/or analysed during the current study are available in supplementary table 1 or in the accompanying 'Source data' file

Field-specific reporting

Please select the one below that is the best fit for your research. If you are not sure, read the appropriate sections before making your selection.

- Life sciences Behavioural & social sciences Ecological, evolutionary & environmental sciences

For a reference copy of the document with all sections, see [nature.com/documents/nr-reporting-summary-flat.pdf](https://www.nature.com/documents/nr-reporting-summary-flat.pdf)

Life sciences study design

All studies must disclose on these points even when the disclosure is negative.

Sample size	No sample size calculation was performed
Data exclusions	No data were excluded
Replication	All experiments were repeated independently at least twice, Each experiment was done with at least two technical replicates
Randomization	Not relevant
Blinding	No blinding was performed

Reporting for specific materials, systems and methods

We require information from authors about some types of materials, experimental systems and methods used in many studies. Here, indicate whether each material, system or method listed is relevant to your study. If you are not sure if a list item applies to your research, read the appropriate section before selecting a response.

Materials & experimental systems

n/a	Involvement in the study
<input checked="" type="checkbox"/>	<input type="checkbox"/> Antibodies
<input type="checkbox"/>	<input checked="" type="checkbox"/> Eukaryotic cell lines
<input checked="" type="checkbox"/>	<input type="checkbox"/> Palaeontology and archaeology
<input checked="" type="checkbox"/>	<input type="checkbox"/> Animals and other organisms
<input type="checkbox"/>	<input checked="" type="checkbox"/> Human research participants
<input checked="" type="checkbox"/>	<input type="checkbox"/> Clinical data
<input checked="" type="checkbox"/>	<input type="checkbox"/> Dual use research of concern

Methods

n/a	Involvement in the study
<input checked="" type="checkbox"/>	<input type="checkbox"/> ChIP-seq
<input checked="" type="checkbox"/>	<input type="checkbox"/> Flow cytometry
<input checked="" type="checkbox"/>	<input type="checkbox"/> MRI-based neuroimaging

Eukaryotic cell lines

Policy information about [cell lines](#)

Cell line source(s)	293T (ATCC CRL-11268) 293T/ACE2cl.22 Exp Med (2020) 217 (11): e20201181. https://doi.org/10.1084/jem.20201181 HT1080/ACE2.cl.14 J Exp Med (2020) 217 (11): e20201181. https://doi.org/10.1084/jem.20201181
Authentication	Not Authenticated after purchase from ATCC
Mycoplasma contamination	Negative for mycoplasma contamination (DAPI staining)
Commonly misidentified lines (See ICLAC register)	<i>Name any commonly misidentified cell lines used in the study and provide a rationale for their use.</i>

Human research participants

Policy information about [studies involving human research participants](#)

Population characteristics	As described previously Wang, Z., Schmidt, F., Weisblum, Y. et al. mRNA vaccine-elicited antibodies to SARS-CoV-2 and circulating variants. Nature 592, 616–622 (2021). https://doi.org/10.1038/s41586-021-03324-6
Recruitment	As described previously: Wang, Z., Schmidt, F., Weisblum, Y. et al. mRNA vaccine-elicited antibodies to SARS-CoV-2 and circulating variants. Nature 592, 616–622 (2021). https://doi.org/10.1038/s41586-021-03324-6
Ethics oversight	Institutional Review Board of the Rockefeller University; protocol DRO-1006

Note that full information on the approval of the study protocol must also be provided in the manuscript.